High-order harmonic generation by chirped and self-guided femtosecond laser pulses. I. Spatial and spectral analysis

V. Tosa,* H. T. Kim, I. J. Kim, and C. H. Nam
Department of Physics, KAIST, Yuseong-gu, Daejeon, 305-701 Korea
(Received 21 October 2004; published 16 June 2005)

For the analysis of high-order harmonics generated in a long gas jet by intense chirped femtosecond laser pulses, calculations of the laser propagation and harmonic generation were performed in terms of a nonadiabatic three-dimensional model. The self-guided propagation, observed at the conditions of bright harmonic generation, was confirmed by the model calculations. When using negatively chirped pulses, the calculated distribution of the harmonic field is spatially and spectrally confined, being generated on axis with a narrow spectral profile. The positively chirped pulses generate broad spectral distribution on axis, and narrow off axis, but in the latter case with a large emission angle. The estimation of harmonic beam divergence agreed well with experimentally measured data, showing the lowest divergence at the conditions of the brightest harmonic generation. Spectral, temporal, and spatial modifications of the propagated laser pulse are found to influence decisively the single-atom response and ultimately the harmonic field, providing a coherent picture of harmonic generation.

DOI: 10.1103/PhysRevA.71.063807 PACS number(s): 42.65.Ky, 42.65.Re

I. INTRODUCTION

Under intense laser irradiation, noble gases generate high-order harmonics in a wide wavelength range. The high-order harmonics are a unique source of extreme ultraviolet/soft x rays, with excellent coherence [1,2], ultrashort pulse duration [3], and continuous wavelength tuning capabilities [4]. Generation of strong radiation requires the application of intense femtosecond laser pulse to a high-density gas medium that is partially ionized during the high-order harmonic generation (HHG). This leads to a defocusing of the laser beam by the electron plasma and hence to a reduction in the driving-field intensity and generation volume. The rapidly ionizing high-density gas medium also modifies the temporal structure of the femtosecond laser pulse due to the self-phase modulation (SPM) [5]. In addition, the spectral structure of high-order harmonics depends critically on the frequency modulation, or chirp, of the driving laser pulses.

Previous experiments using chirped femtosecond pulses [6–8] have shown that the spectral structure of harmonics varies sensitively to the applied laser chirp. At relatively low laser intensity, individual harmonic peaks are well defined and discrete for positively chirped (PC) pump pulses, while the harmonic spectra merge to become a continuum for negatively chirped (NC) pump pulses. These spectral features are effects of the single-atom phase of the generated harmonic emission, and can be reduced or enhanced by applying a negative or positive chirp to the laser frequency, respectively. In this case, dynamically induced harmonic chirps could be compensated for by PC laser pulses and the effect of ionization on HHG was not significant. However, when ionization induces a significant SPM in the leading edge of the pulse [7], the behavior is quite contrary: the NC pulses induce a strong harmonic emission, while with PC pulses the harmonic spectra in the plateau became weaker and broader. Using a one-dimensional model for the analysis of pulse propagation and HHG, it was concluded that the SPM-induced positive chirp is chiefly responsible for this behavior as it can be large enough to overcompensate the dynamically induced negative chirp.

The technique of using chirped pulses was recently applied to HHG optimization experiments [4,7,9]. The optimization processes in both space and time domains [9] maximized the harmonic generation volume by inducing a profile-flattened, self-guided regime of beam propagation, and allowed the generation of spectrally sharp harmonics by adding appropriate chirp to the laser frequency. The optimization of the emission volume was accomplished by placing the jet about one Rayleigh length (z_R) before the focus while the brightness maximization was obtained by applying negatively chirped pulse. To gain a detailed understanding of the HHG processes under these optimized conditions, we performed a systematic analysis through extensive numerical modeling.

Our approach uses a nonadiabatic three-dimensional (3D) model [10] for the propagation of both the driving field as well as the harmonic field. The results of our modeling are in good agreement with the experimental results and thus enable us to explain the observed features and to reveal the underlying physics. First, using experimental parameters (focusing geometry, pulse energy, frequency, and duration) as input data for our model, we could quantitatively reproduce the formation of the self-guiding of the fundamental beam. The obtained results are in agreement with measured quantities such as the axial distribution of the plasma fluorescence and the radial profile of the laser intensity. Second, the spatial and spectral distribution of the generated harmonics could be predicted by the calculated harmonic field. In particular, our calculations show that, when using NC pulses, the distribution of the harmonic field is both spatially and

*On leave from the National Institute for R&D in Isotopic and Molecular Technologies, Cluj-Napoca, Romania.

spectrally confined, being generated on axis and with sharp spectral profile. The positive chirp in the fundamental pulse generates a broad spectral distribution on axis, and sharper off axis, but in this case with higher spatial divergence. Our analysis shows that the single-atom emission will depend crucially on the modifications suffered by the driving field during propagation. The spatial, spectral, and temporal modifications suffered by the laser pulse are used to explain harmonic field characteristics through the single-atom response. Furthermore, the phase matching between the laser pulse and generated harmonics also plays a role by selecting particular trajectories that survive and contribute to the final harmonic field. The present paper deals with spatial and spectral characteristics of the generated harmonics. The time-frequency analysis of the single-atom response and of the harmonic field, as well as the time-dependent phase-matching calculations are presented in the following article of this issue [11], hereafter referred to as II.

The paper is organized as follows: in Sec. II we describe the essentials of our experiment and explain the numerical model used for calculating the fundamental and harmonic field propagation. Characteristic experimental results as well as the results of the modeling are presented in Sec. III. By corroborating these results we are able to coherently explain our data and reveal the underlying physical processes. Conclusions are presented in Sec. IV.

II. EXPERIMENT AND MODELING

High-order harmonic experiments were carried out using a long gas jet driven by intense femtosecond Ti:sapphire laser pulses. In the experiments, femtosecond laser pulses of variable duration and chirp with wavelength centered at 827 nm were focused using a spherical mirror ($f=1.2$ m) onto a long neon gas jet produced with a 9 mm slit nozzle. The peak gas density was about 40 Torr, a value that was established in the optimization process. The measured beam waist at the laser focus was 72 μm [full width at half-maximum (FWHM)], reaching a peak laser intensity of 2×10^{15} W/cm^2. To examine the laser propagation through the gas medium, a visible plasma image was recorded by a charge-coupled-device (CCD) detector. The intensity profile of the laser beam at the exit position of the gas jet was directly measured using an image-relaying lens and a CCD. The harmonics generated were detected by a flat-field soft x-ray spectrometer equipped with a back-illumination x-ray CCD. More details about the experiments can be found in [9,12].

The 3D nonadiabatic model for pulse propagation and harmonic generation was described in detail in [13], so that we recall here only the main features. In an ionized gas, the pulse evolution is described by the wave equation

$$\nabla^2 E_1(r,z,t) - \frac{1}{c^2}\frac{\partial^2 E_1(r,z,t)}{\partial t^2} = \frac{\omega_0^2}{c^2}(1-\eta_{eff}^2)E_1(r,z,t), \quad (1)$$

where $E_1(r,z,t)$ is the axially symmetric transverse electric field of frequency ω_0. The effective refractive index of the medium was written as: $\eta_{eff}(r,z,t)=\eta_1(r,z,t)+\eta_2 I(r,z,t)-\omega_p^2(r,z,t)/2\omega_0^2$. The linear term $\eta_1=1+\delta_1-i\beta_1$ accounts for the dispersion (δ_1) and absorption (β_1), while the second term describes the optical Kerr effect. The third term contains the plasma frequency $\omega_p=(4\pi e^2 n_e/m)^{1/2}$ and accounts for the presence of a density n_e of electrons per unit volume. The free electron concentration was calculated using the Amosov-Delone-Krainov formula [14]. We used a Fourier transform method to solve the above equation, as described in [15], combined with a standard Cranck-Nicholson scheme in space. It should be stressed that, to set the initial conditions for the above differential equation, we used the *measured* energy of the pulse, assuming a Gaussian beam in space and time with *measured* beam waist and pulse duration.

For the harmonic field calculation, the single-atom response, estimated in the strong-field approximation formalism [16], is the source term for the 3D propagation equation

$$\nabla^2 E_h(r,z,t) - \frac{\eta^2}{c^2}\frac{\partial^2 E_h(r,z,t)}{\partial t^2} = \mu_0\frac{\partial^2 P_{nl}(r,z,t)}{\partial t^2}, \quad (2)$$

where $P_{nl}(r,z,t)=[n_a(z)-n_e(r,z,t)]d_{nl}(r,z,t)$ is the nonlinear polarization of the gas generated by the nonlinear dipole moment $d_{nl}(r,z,t)$ of the single atom, and $n_a(z)$ the initial atomic density. In this equation, the refractive index η takes into account the atom dispersion and absorption but ignores free electron dispersion because the plasma frequency is much lower than the frequencies of high-order harmonics.

In modeling the fluorescence signal, the basic assumption we make is that the observed fluorescence originates from the ions, and therefore consider its intensity to be proportional to the local ion concentration. In addition, we assume that this ion concentration is equal to the electron concentration $n_e(r,z,\tau_p)$ at the end of the laser pulse. The total fluorescence signal along the propagation direction, $S(z)$, can be linked to the radially integrated electron concentration

$$S(z) \sim \int n_e(r,z,\tau_p) r dr \quad (3)$$

over the interaction region. We used the rational function $y=ax/(b+cx)$ to account for the decreasing gas density for 1 mm at both jet ends.

III. RESULTS AND DISCUSSION

A. Laser propagation

The propagation of the laser pulse was calculated using parameters that mimic our optimized experimental conditions as closely as possible. As described in [9], the optimum harmonic emission was obtained by placing the long gas jet at a distance $z_0 \approx -z_R$ in the converging beam. The formation of a long plasma filament was observed under optimized conditions. This filament became shorter as the gas jet moved toward the focus. Figure 1 gives the profile of the total fluorescence intensity along the propagation direction, and the integrated electron concentration, calculated by solving Eq. (1), for a 42 fs pulse with energy of 4.8 mJ propa-

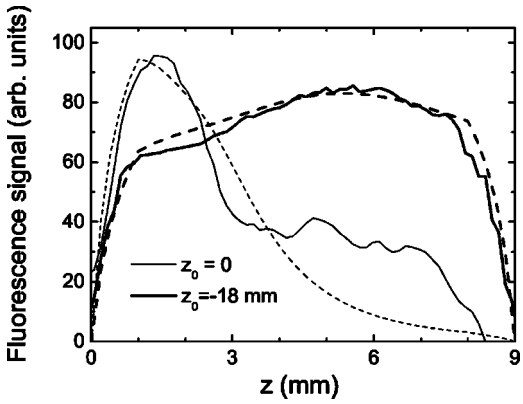

FIG. 1. Fluorescence intensity observed along the gas jet for two different jet positions: $z_0=0$ and $z_0=-18$ mm. Dotted lines represent the integrated electron concentration, as described in the text.

gating in Ne at 40 Torr. The agreement between the experimental and calculated results was very good for the jet placed at $z_0=-18$ mm. For $z_0=0$ the agreement was satisfactory in the first few millimeters of propagation, but became poorer for longer distances, which suggests a nonhomogeneous propagation of the beam due to the high degree of ionization. Indeed, when the jet is positioned at the focus, a 5 mJ laser pulse causes almost full ionization in the central part ($r \lesssim 20$ μm) of the beam.

The formation of profile flattening of the propagating laser beam is clearly seen for the gas jet position $z_0=-18$ mm. Figure 2 shows the calculated spatial profile of the laser intensity along the gas jet at the time of the pulse peak. After an initial decrease caused by defocusing, the on-axis intensity remains nearly constant at about 5.5×10^{14} W/cm^2 for distances ranging from $z\simeq2.5$ mm to the rest of the propagation distance considered, up to 15 mm. When this happens, the radial profile of the intensity becomes nearly flattop with a FWHM diameter of 140 μm, which is increased to 190 μm after 9 mm of propagation. One can also note from Fig. 2 that the flattop profile gradually decays with further propagation. This field configuration could be obtained only for the jet placed in the convergent

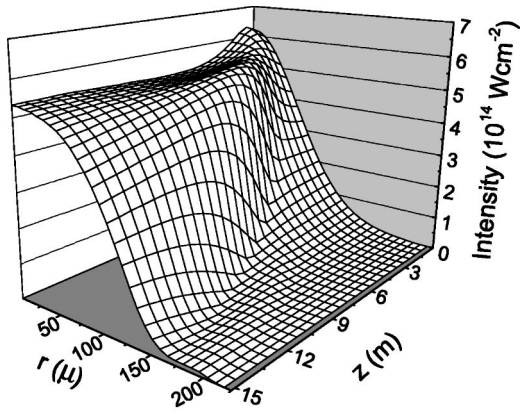

FIG. 2. Spatial configuration of the laser intensity profile calculated for the jet position $z_0=-18$ mm. Propagation was extended to 15 mm to evidence the gradual decay of the self-guided mode.

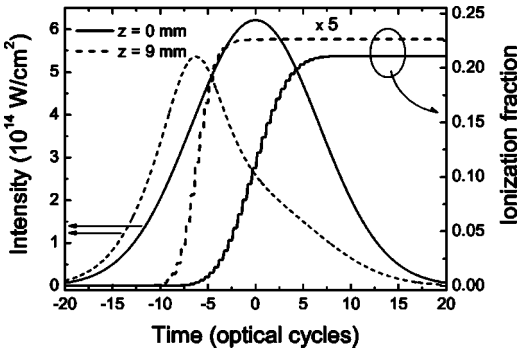

FIG. 3. Time dependence of the on-axis laser intensity and ionization fraction at $z=0$ (solid lines) and $z=9$ mm (dashed lines). For comparison purpose the ionization fraction for $z=9$ mm is enlarged five times. Other conditions: Ne, 40 Torr, 9 mm long jet placed at $z_0=-18$ mm, Rayleigh length $z_R=18$ mm.

beam, i.e., before the focus. If the jet is placed after the focus, the intensity decreases in both axial and radial directions due to the cumulative effects of plasma defocusing and initial beam divergence.

We clearly identified the self-guided propagation in the 9-mm jet by observing in the near field the profile flattening of the laser intensity at the exit position of the gas jet [9]. The spatial profile of the laser intensity showed good agreement with the calculation. It clearly showed the flattening in the central part (see Fig. 2 of [9]), with a FWHM diameter of about 180 μm.

When the laser pulse enters a gas medium, the ionized medium at the entrance region acts like a diverging lens with decreasing focal power as r increases. The medium thus changes the radius of curvature of the converging laser beam, more in the central and less in the peripheral regions, so that a flattened laser intensity profile is formed. The electron concentration then follows this profile; however, due to the strong nonlinear dependence of ionization rate on laser intensity, this concentration decreases sharply at the plasma boundary, by 1 order of magnitude over a 10 μm scale. Unlike the common self-guiding effect, wherein the field confinement is due to the total internal reflection at guide boundaries, the effect here is obtained due to the reflection of the trapped wave from the plasma boundary that is sharp compared to the transverse scale. The propagation of this field configuration lasts for a distance of about one Rayleigh length, enough for the HHG process to take place in homogeneous conditions of intensity and phase for the pump field. We mention that the formation of a self-guided beam was indirectly observed previously in a static cell by measuring the axial [10] and transversal [13] plasma fluorescence. In addition, a flattening of the central beam was observed [17] in a 1 mJ, 200 fs pulse propagation in air and found to be detrimental for obtaining enough laser intensity needed for materials processing.

We also analyzed the temporal distortions of the laser pulse during propagation, as these distortions directly influence the harmonic generation. Figure 3 shows the time dependence of the laser intensity and ionization fraction at the beginning ($z=0$) and the end ($z=9$ mm) of the interaction region. For the conditions specified in Fig. 3, the trailing part

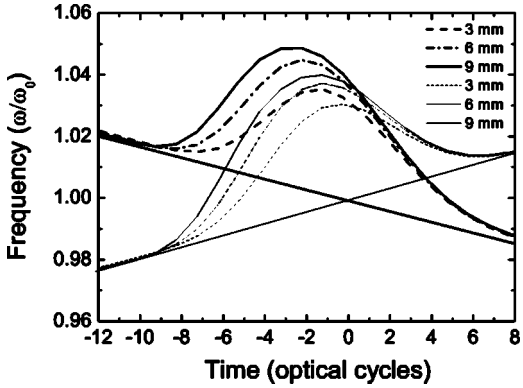

FIG. 4. Instantaneous frequency for PC and NC pulses after 3, 6, and 9 mm of propagation. Other conditions are as in Fig. 3. The SPM effect is strongest in the first 3 mm, where ionization is maximum.

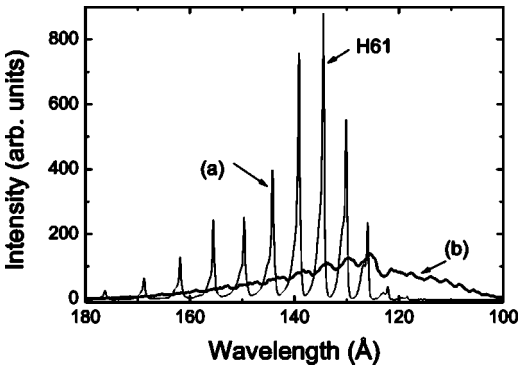

FIG. 5. Harmonic spectra from Ne driven by femtosecond laser pulses with different laser chirps: (a) NC 42-fs and (b) PC 41-fs laser pulses.

of the laser pulse interacts with the generated plasma and is shortened from 42 fs to about 30 fs, in addition to the shift in time of the pulse peak toward the leading edge of the pulse (in the moving reference frame). The ionization dynamics is also modified: the ionization profile shortens duration and moves toward earlier times. The effective refractive index η_{eff} follows the jump of the electron concentration, decreasing from $\eta_{eff} \gtrsim 1$ to $\eta_{eff} < 1$ due to the dominant contribution of the electron plasma over the neutral contribution. The Kerr contribution to the refractive index is also small compared to the electron contribution. Therefore, the plasma-induced defocusing dominates over the effects of self-focusing and group velocity dispersion. This holds for both PC and NC laser pulses, and similar pulse shortening was observed for both cases. A numerical study on the propagation of a 100 fs pulse in Ar at 1 atm pressure also reported the pulse shortening and shifting to earlier time, due mainly to plasma defocusing [18].

Our modeling studies show that, for the same absolute value of laser chirp, both PC and NC pulses generate the same spatial map of the laser intensity. For the same absolute chirp value we assumed the same pulse duration, an assumption that is very close to the experimental facts. Under these conditions the ionization rates are practically identical, so that the two pulses propagate under identical conditions. However, the way in which plasma-induced SPM affects the temporal characteristics of the two oppositely chirped pulses leads to different conditions for the dipole emission from target atoms and, subsequently, for harmonic generation. As we shall see in the following, this crucially influences the single-atom response and ultimately the characteristics of the harmonics.

Detailed time/frequency features of the laser pulse passing through the medium can be revealed by the Wigner distribution function [19], which simultaneously describes the temporal and spectral behavior of ultrashort laser pulses. It also allows us to calculate the instantaneous frequency of the field, which is presented in Fig. 4 for both PC and NC pulses. Due to the SPM induced in the ionizing medium, the laser frequency increases with time (the chirp becomes positive even for the NC pulse) in the leading edge, and then decreases (gaining a negative chirp) back to the linear frequency variation. The SPM effect per unit length of propagation is strongest in the first 3 mm of propagation, where the ionization rate is high. In the self-guided region, SPM increases steadily with propagation distance, due to the presence of a nearly constant concentration of electrons. By comparing the data for $z=9$ mm in Figs. 3 and 4 one can note that the rise of the ionization fraction coincides with the increase of the carrier frequency of the fundamental. In other words, for both pulses the dipole emission takes place when their frequency has a positive chirp.

B. Harmonic generation

In order to gain a realistic picture of the HHG process, we performed a series of simulations with laser chirp and energy as the main scan parameters. From the large amount of data obtained, we focus our discussion on two specific cases, namely, modeling HHG for PC and NC 42-fs Gaussian pulses of same energy, all other conditions being those specified in Fig. 3. The absolute value of the chirp was taken from experiment as 8×10^{-4} fs^{-2} for the two pulses. The two measured spectra corresponding to these two cases are shown in Fig. 5. The gas jet was placed at $z=-18$ mm. As is shown, the NC 42 fs pulse generated sharp and strong radiation around the 61st harmonic (H61), while the PC 41-fs pulses produced a quasicontinuous harmonic spectrum.

Once the solution $E_1(r,z,t)$ for the propagating the laser electric field was obtained, the single-atom source, calculated in every grid point of the interaction region, was used to solve the propagation equation [Eq. (2)] for the harmonic field. The solution, $E_h(r,z,\omega)$, allows a detailed characterization of the HHG mechanism, both in space and in time/frequency. In the following we analyze the harmonic fields generated by PC and NC pulses, which have the same spatial configuration of the driving field but opposite initial chirp values. To estimate the influence of chirp on the spatial configuration of the harmonic field, we plotted the (r,z) map of H61 intensity, as shown in Fig. 6, for the same laser energy of 5 mJ but for different initial chirps. The chirp values are 6×10^{-4}, 8×10^{-4}, and 10^{-3} fs^{-2}, for 35-, 42-, and 50-fs pulses, respectively. For this calculation we considered a 15

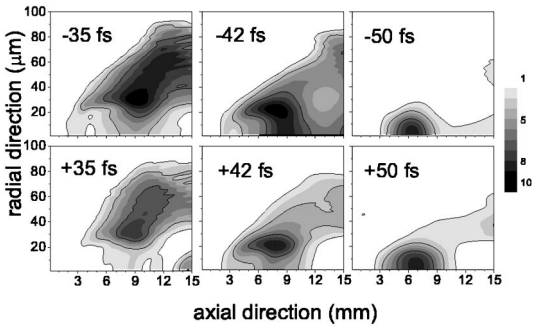

FIG. 6. Spatial map of H61 relative intensity from a 15 mm long jet of Ne driven by chirped pulses. The laser energy and gas pressure were 5 mJ and 40 Torr, respectively. The sign and duration of chirped pulses are given in the figure.

mm long jet in order to obtain an estimation of the optimum pressure and harmonic generation volume, based on the H61 buildup. Indeed, for 40 Torr gas pressure and a 42 fs laser pulse, the maximum H61 field is observed after about a 9 mm propagation, as shown in Fig. 6. This is in agreement with the experimental results, which show that the highest brightness obtained using a 9 mm neon gas jet and NC 42 fs pulse was for 40 Torr. On the other hand, the PC 42 fs pulse generates the maximum H61 also after a 9 mm propagation, but at off axis, and the generation volume is smaller. Decreasing the chirp, i.e., using 35-fs pulses with a 6×10^{-3} fs^{-2} chirp, does not modify the optimal jet length for maximal emission, but the maximum field is formed at off axis. Still, the NC pulse induces a stronger harmonic field. Increasing the duration and chirp to 50 fs and 10^{-2} fs^{-2}, respectively, the two maps are rather similar for $z\lesssim9$ mm. This behavior was also observed experimentally, the spectra obtained from PC and NC pulses with increased duration do not differ too much. There is a slightly better H61 field for the PC pulses, as the ionization effects are diminished, and a decrease of the optimal length to about 6 mm. In similar data that we obtained for different pulse energies, we noted that the pulse energy and the pulse chirp produce opposite effects: a higher pulse energy will enhance the SPM effect, which will be balanced by a higher initial chirp. Therefore, the pattern observed in Fig. 6, at 5 mJ and for ±42-fs pulses, roughly translates to ±50 fs at 6 mJ, and to ±35 fs at 4 mJ. The HHG optimization aiming a spectral brightness maximization was obtained by making use of this balance between initial chirp and SPM. For given parameters that determine the SPM magnitude, such as working pressure, pulse energy, and jet position, the optimization can be achieved by finely tuning the initial pulse chirp.

The differences between the harmonic fields generated with PC and NC pulses of 42 fs can be seen in Fig. 7, where we have plotted the near field of the harmonics around H61 as a function of frequency and radial coordinate. The PC case (upper panel in Fig. 7) shows a diffuse spectral profile near the axis and a sharper one between 40 and 70 μm. On the contrary, the NC pulse produces a clean spectral profile in the compact central region extending up to about 40 μm. The present result together with the result presented in Fig. 6 demonstrate an optimization of the generation volume for

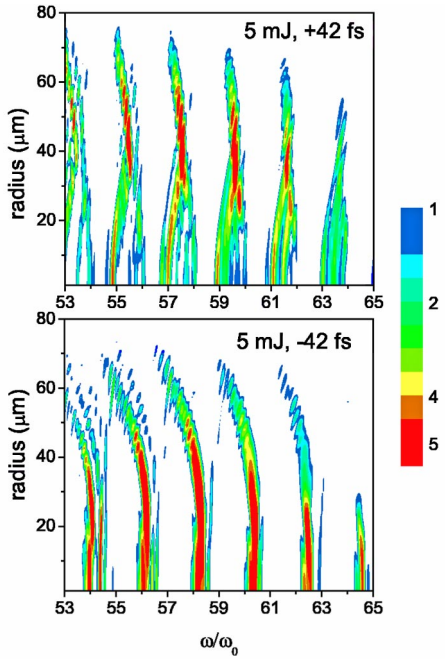

FIG. 7. (Color online) Radial and frequency dependence of the harmonic field intensity at $z=9$ mm, for PC (upper panel) and NC (lower panel) 42-fs pulses. Logarithmic scale, arbitrary units.

our specific conditions of initial pulse energy and chirp.

The mechanism behind this behavior must be searched for by starting from the single-atom response to the driving field. The time-frequency analysis of the single-atom response, as shown in II, reveals that the dipole emission around H61 frequency develops basically during the rise of the ionization front. In particular, for 42-fs pulses and on axis, the harmonic emission occurs between −10 and −2 optical cycles measured from the center of the initial pulse (see Fig. 3). This range coincides with the time of a strong positive chirp induced by SPM to the laser pulses of both PC and NC pulses. The single-atom calculation (see Figs. 2 and 3 in II) also shows that strong harmonic emission occurs during the decreasing part of the driving field, right after the peak. The interaction intensity is in the range $(4.0-4.5)\times10^{14}$ W/cm^2, which places H61 close to the cutoff of the generated harmonics. Earlier studies [20] on HHG in a rapidly ionizing medium also found that the harmonic radiation in the cutoff is generated during the period of rapid ionization, which may not coincide with the peak of the laser pulse.

The spectral features of the single-atom response inherit the spectral features of the driving field that is distorted during its propagation through a rapidly ionizing medium. Analysis of the instantaneous laser frequency in the self-guided region shows that the frequency modulation, while preserving the form shown in Fig. 4, diminishes its amplitude with increasing r but with a smaller rate close to on axis and a higher rate in the peripheral regions. For PC pulses, the total chirp of the driving field overcompensates the harmonic intrinsic chirp for $r\lesssim30-40$ μm and induces a broad dipole response that is also positively chirped. For larger r, the single-atom emission diminishes its chirp and spectral width

because the laser chirp decreases and can balance the dynamically induced harmonic chirp. For the conditions considered here this happens for $r>40$ μm, which explains the off-axis formation of a spectrally well-defined harmonic field. On the other hand, the NC pulses have, during dipole emission, a smaller total chirp that can balance the intrinsic harmonic chirp. This balance is maintained well in the central part of the self-guided region because of the small radial variation of the SPM, which provides the condition for homogeneous harmonic emission in the central region.

Figure 7 shows an interesting feature of a redshifted tail that extends from $r=40$ to $r=70$ μm in the case of the NC pulse. This tail is clearly present also in the experimental result (see Fig. 5) as an asymmetric spectral profile of each harmonic generated by the NC pulses. The redshift of the harmonic profile in Fig. 7 comes from the fact that the SPM effect is weaker for larger r due to smaller ionization. In addition the strong harmonic emission occurs at the time of the negative chirp part, i.e., after the highest instantaneous laser frequency (around −2 optical cycles in Fig. 3). Thus, the emission frequency decreases with increasing r, producing the redshifted tail in the harmonic spectrum. Consequently, the present results clearly identify the origin of the experimentally observed asymmetric harmonic profile.

The behavior of harmonics generated by the PC pulse has different spatial characteristics from that by the NC pulse. For the case of the PC pulse in Fig. 7, a spectrally sharp field is generated around 40 μm, although the on-axis harmonic field is broad. This indicates that the spectra generated in the far field could contain also well-defined harmonic peaks. To clarify this point we also calculated the beam divergence of the harmonics at the exit of the interaction region, i.e., at $z=9$ mm. This was done by taking advantage of the fact that the final solution for the propagation equation is obtained in the spectral domain, which allows the calculation of the phase derivatives (wave vectors) both in radial $k_r=\partial\varphi/\partial r$ and in axial $k_z=\partial\varphi/\partial z$ directions. Therefore, the component $E_h(\omega)$ of the field makes an angle α with the z axis, where $\tan(\alpha)=k_r/(k_z+\omega/c)$. The full emission angle (2α) calculated in this way is given in Fig. 8, for the harmonics plotted in Fig. 7. As one can see, on axis and for small radii, both PC and NC cases develop highly collimated harmonics, with a total divergence less than 0.5 mrad. This favors the NC case, as it allows the propagation of sharp harmonics near the axis with small divergence. For the PC case, the spectrally broad field near the axis can propagate with low divergence, but spectrally well-defined harmonics at off axis propagate with large divergence, generating only a weak signal. This is consistent with the experimentally observed harmonic spectrum of the PC laser pulse shown in Fig. 5

The harmonic beam divergence at different laser chirps was calculated and compared with experimental measurements. From the far-field profiles we measured the divergence of H61 for different chirp conditions of the laser pulse, all other parameters being maintained constant and specified in Fig. 3. From the modeling, a theoretical value of the H61 divergence was also obtained as a weighted average of the divergence angle presented in Fig. 8, within the frequency range of H61. The weighting factors are taken from the corresponding H61 intensities plotted in Fig. 7. The data on H61

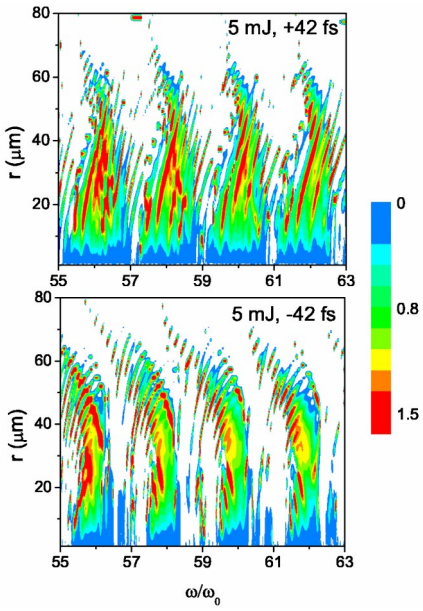

FIG. 8. (Color online) Radial and frequency dependence of the harmonic field divergence (full angle) at $z=9$ mm, for PC (upper panel) and NC (lower panel) 42-fs pulses. Linear scale from 0 to 1.5 mrad.

divergence, presented in Fig. 9, clearly show good agreement between the calculated and measured harmonic divergence. The minimum divergence was observed at the condition of the maximum of harmonic brightness, i.e., for NC 42-fs pulses, as a consequence of profile flattening and chirp compensation mechanism. We must mention that at extremal positions of the grating, where the absolute value of the chirp does not increase but only the pulse duration increases, the increase in divergence (for both PC and NC pulses) is due mainly to a lower driving-field intensity, which leads to different harmonic emission conditions. The calculation performed using a pulse duration of 75 fs and a negative chirp of 5×10^{-4} fs^{-2} (corresponding to a grating separation of +350 μm in Fig. 9) shows that the profile flattening is no longer present because the initial laser intensity is too

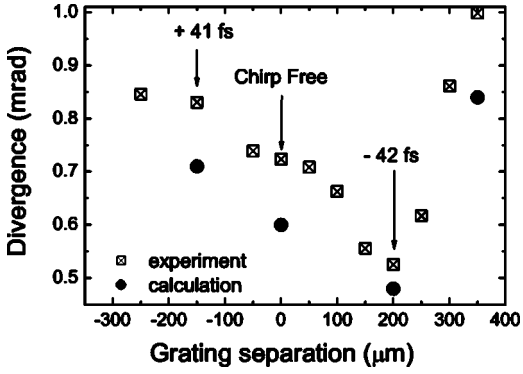

FIG. 9. H61 divergences obtained at the conditions specified in Fig. 3.

low to create the minimum electron density [10] necessary for self-guiding ignition. In addition, the increase of the divergence, even for ±50-fs cases (about ±250 μm in Fig. 9) is due to the fact that the harmonic emission is no longer optimized for the 9 mm jet, as shown in Fig. 6. Consequently, the good agreement between the calculated and observed harmonic divergences also supports the current 3D calculation of laser propagation and high-order harmonic generation and propagation.

IV. CONCLUSIONS

Using a nonadiabatic 3D model for the propagation of intense chirped laser pulses and harmonic generation, we analyzed the spatial, spectral, and temporal characteristics of the laser pulse and of the generated harmonics. The calculated results showed good agreement with experimental data: (i) the image of the observed plasma fluorescence was qualitatively reproduced by the electron density profile along the propagation direction, (ii) the beam profile of the laser pulse measured at the exit of the gas jet was reproduced directly in the calculation of the propagated field, and (iii) the results of the model, concerning the spectral and spatial structure of the harmonic field, allowed us to explain the observed features of the harmonic spectra generated by positively and negatively chirped pulses. The analysis of the detailed mechanism of harmonic field enhancement, starting from the single-atom response, was performed and is presented in the next article [11].

The spatial, temporal, and spectral characteristics of the driving laser, during its propagation in an ionizing medium, were estimated, as they proved to influence critically the harmonic generation. The detailed analysis revealed the self-guiding of the laser beam, which creates a profile-flattened central region. This is very favorable for HHG, as it provides rather large volumes of constant intensity and phase for the driving field. The temporal modifications of the laser pulse, peak shift toward the leading edge and pulse shortening due to electron plasma, are translated into modifications of the single-atom emission time. In addition, the plasma-induced SPM modifies the initial chirp and affects in a crucial way the spectral response of the single atom and further on the overall harmonic field. We found that the pulses with initial negative chirp produce harmonics with a narrow spectral profile in a compact volume around the propagation axis. The pulses with an initial positive chirp generated harmonics with weaker and broader spectral distribution on axis. Taking into account the above factors influencing HHG processes, we can develop a coherent picture of the processes behind the experimentally observed spectra.

ACKNOWLEDGMENTS

The research was supported by the Ministry of Science and Technology of Korea through the Creative Research Initiative Program. V.T. acknowledges support from KOSEF Brain Pool Program.

[1] R. A. Bartels, A. Paul, H. Green, H. C. Kapteyn, M. M. Murnane, S. Backus, I. P. Christov, Y. Liu, D. Attwood, and C. Jacobson, Science **297**, 376 (2002).
[2] D. G. Lee, J. J. Park, J. H. Sung, and C. H. Nam, Opt. Lett. **28**, 480 (2003).
[3] M. Paul, E. S. Toma, P. Breger, G. Mullot, F. Auge, Ph. Balcou, H. G. Muller, and P. Agostini, Science **292**, 1689 (2001).
[4] H. T. Kim, D. G. Lee, K.-H. Hong, J.-H. Kim, I. W. Choi, and C. H. Nam, Phys. Rev. A **67**, 051801(R) (2003); H. J. Shin, D. G. Lee, Y. H. Cha, K. H. Hong, and C. H. Nam, Phys. Rev. Lett. **83**, 2544 (1999).
[5] J. H. Kim and C. H. Nam, Phys. Rev. A **65**, 033801 (2002).
[6] Z. Chang, A. Rundquist, H. Wang, I. Christov, H. C. Kapteyn, and M. M. Murnane, Phys. Rev. A **58**, R30 (1998).
[7] D. G. Lee, J.-H. Kim, K.-H. Hong, and C. H. Nam, Phys. Rev. Lett. **87**, 243902 (2001).
[8] T. Sekikawa, T. Ohno, T. Yamazaki, Y. Nabekawa, and S. Watanabe, Phys. Rev. Lett. **83**, 2564 (1999).
[9] H. T. Kim, I. J. Kim, D. G. Lee, K. H. Hong, Y. S. Lee, V. Tosa, and C. H. Nam, Phys. Rev. A **69**, 031805(R) (2004).
[10] V. Tosa, E. Takahashi, Y. Nabekawa, and K. Midorikawa, Phys. Rev. A **67**, 063817 (2003).
[11] V. Tosa, H. T. Kim, I. J. Kim, and C. H. Nam, following paper, Phys. Rev. A **71**, 063808 (2005).
[12] H. T. Kim, I. J. Kim, V. Tosa, Y. S. Lee, and C. H. Nam, Appl. Phys. B: Lasers Opt. **78**, 863 (2004).
[13] E. Takahashi, V. Tosa, Y. Nabekawa, and K. Midorikawa, Phys. Rev. A **68**, 023808 (2004).
[14] M. V. Amosov, N. B. Delone, and V. P. Krainov, Zh. Eksp. Teor. Fiz. **91**, 2008 (1986).
[15] E. Priori, G. Cerullo, M. Nisoli, S. Stagira, S. De Silvestri, P. Villoresi, L. Poletto, P. Ceccherini, C. Altucci, R. Bruzzese, and C. de Lisio, Phys. Rev. A **61**, 063801 (2000)
[16] M. Lewenstein, Ph. Balcou, M. Yu. Ivanov, A. L'Huillier, and P. B. Corkum, Phys. Rev. A **49**, 2117 (1994).
[17] J. Sun and J. P. Longtin, J. Opt. Soc. Am. B **21** 1081 (2004).
[18] M. Mlejnek, E. M. Wright, and J. V. Moloney, Phys. Rev. E **58**, 4903 (1998).
[19] J. H. Kim, D. G. Lee, H. J. Shin, and C. H. Nam, Phys. Rev. A **63**, 063403 (2001).
[20] S. C. Rae, K. Burnett, and J. Cooper, Phys. Rev. A **50**, 3438 (1994).